THE JOURNAL OF PHYSICAL CHEMISTRY B
A JOURNAL OF THE AMERICAN CHEMICAL SOCIETY

pubs.acs.org/JPCB

Article

Lysine-Dependent Entropy Effects in the *B. subtilis* Lysine Riboswitch: Insights from Single-Molecule Thermodynamic Studies

Andrea Marton Menendez and David J. Nesbitt*

Cite This: https://doi.org/10.1021/acs.jpcb.1c07833

Read Online

ACCESS | Metrics & More | Article Recommendations | Supporting Information

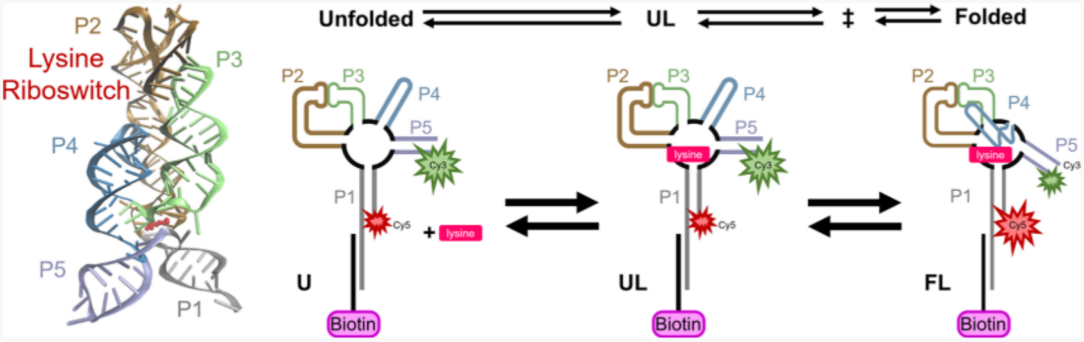

ABSTRACT: Riboswitches play an important role in RNA-based sensing/gene regulation control for many bacteria. In particular, the accessibility of multiple conformational states at physiological temperatures allows riboswitches to selectively bind a cognate ligand in the aptamer domain, which triggers secondary structural changes in the expression platform, and thereby "switching" between on or off transcriptional or translational states for the downstream RNA. The present work exploits temperature-controlled, single-molecule total internal reflection fluorescence (TIRF) microscopy to study the thermodynamic landscape of such ligand binding/folding processes, specifically for the *Bacillus subtilis* lysine riboswitch. The results confirm that the riboswitch folds via an induced-fit (IF) mechanism, in which cognate lysine ligand first binds to the riboswitch before structural rearrangement takes place. The transition state to folding is found to be enthalpically favored ($\Delta H_{fold}^{\ddagger} < 0$), yet with a free-energy barrier that is predominantly entropic ($-T\Delta S_{fold}^{\ddagger} > 0$), which results in folding (unfolding) rate constants strongly dependent (independent) of lysine concentration. Analysis of the single-molecule kinetic "trajectories" reveals this rate constant dependence of k_{fold} on lysine to be predominantly entropic in nature, with the additional lysine conferring preferential advantage to the folding process by the presence of ligands correctly oriented with respect to the riboswitch platform. By way of contrast, van't Hoff analysis reveals enthalpic contributions to the overall folding thermodynamics (ΔH^0) to be surprisingly constant and robustly independent of lysine concentration. The results demonstrate the crucial role of hydrogen bonding between the ligand and riboswitch platform but with only a relatively modest fraction (45%) of the overall enthalpy change needed to access the transition state and initiate transcriptional switching.

I. INTRODUCTION

Riboswitches constitute important regulatory elements widely exploited in bacterial and some eukaryotic RNA, composed of an aptamer and expression platform, and typically found in the untranslated regions upstream of the gene they have evolved to regulate.[1−7] The aptamer recognizes and binds a specific ligand and will fold to encapsulate it.[8] In doing so, the aptamer changes the secondary structure of the riboswitch expression platform, which can force RNA polymerase to halt transcription of the gene.[9] Thus, by binding of its cognate ligand, the riboswitch can switch between transcriptionally "active" or "inactive" conformations to enhance or inhibit gene expression. Riboswitches abound in nature, with demonstrated sensitivities to a wide variety of ligand types such as ions, metal cations, cofactors, and amino acids,[10−14] each tailored to recognize and bind their ligand with exquisite specificity.[15−18] To achieve this level of ligand identification, secondary structural motifs in riboswitches fold to form complex binding pockets, whose exposed internal contacts interact with high selectivity for ligand functional groups of the correct size and shape.[8,19−21] This remarkable level of ligand selectivity and recognition offers novel opportunities for riboswitches in diverse sensing

Received: September 3, 2021
Revised: December 10, 2021

applications[22−24] as well as use in the development of antimicrobial therapeutics.[25−30]

The diversity of RNA motifs available to riboswitches lends itself to a variety of folding pathways,[31−34] with binding often described by the two kinetic limits of (i) induced-fit (IF) or (ii) conformational selection (CS) process. In induced-fit (IF) systems, the ligand first binds to the RNA aptamer domain before subsequent folding changes take place to stabilize the tertiary structure. This contrasts with conformational selection (CS) events, where the RNA folds first to form a competent aptamer binding domain to which the ligand then subsequently binds and stabilizes.[35−37] Although these mechanisms obviously represent only two limiting paradigms in a potentially more complex kinetic framework, they do provide well-established paradigms for binding/folding, thus determining the most important factors impacting riboswitch biochemical dynamics.

In this regard, single-molecule fluorescence resonance energy-transfer (FRET)[38,39] experiments have proven especially useful in identifying and highlighting such IF and CS pathways,[35,40,41] particularly when exploited to investigate riboswitch folding vs unfolding kinetics as a function of temperature, ligand, and cation conditions. By way of example, a cognate ligand can often be shown to stabilize the overall folded conformation of the riboswitch upon binding,[16] but this does not by itself distinguish between CS and IF. However, whether the overall folding rate kinetic process is accelerated with enhanced ligand concentration can help distinguish between these two, with, for example, the presence or absence of a strong ligand dependence on k_{fold} signaling either an induced-fit (IF) or conformational selection (CS) mechanism, respectively. In particular, temperature-dependent rate and equilibrium constant data provide qualitatively new insights into the underlying thermodynamics, e.g., revealing at what point(s) along folding reaction coordinate (e.g., pre- or post-transition state) that enthalpic vs entropic contributions play the more predominant role in conformational change and stabilization. Indeed, it is the detailed elucidation of such kinetic, thermodynamic, and mechanistic issues in the *Bacillus subtilis* lysine riboswitch that serves as the primary focus of the present work.

The aptamer binding domain for the *B. subtilis* lysine riboswitch is a five-way helical junction whose constituents interact in a variety of motifs to create a binding pocket for the cognate lysine ligand.[1,11,20,21,42,43] Although some tertiary structure is preformed, the riboswitch undergoes further rearrangement upon interacting with lysine. Crucially, the riboswitch binds lysine from an unfolded (apo) state into a lysine-bound (holo) state, which, in turn, triggers conformational changes such that the helices come together to envelop the ligand in a fully folded state. To simplify matters, we have restricted our studies to a minimal construct (see Figure 1), which formally monitors the relative positions of P1 and P5, but has been demonstrated to recapitulate ligand-induced binding and folding of the riboswitch.[33,44] Furthermore, previous work has shown that lysine facilitates aptamer folding via an induced-fit (IF) mechanism,[44,45] with lysine (L) first binding to the unfolded riboswitch (U) before subsequent folding (U → F) of the riboswitch tertiary structure can occur, i.e.

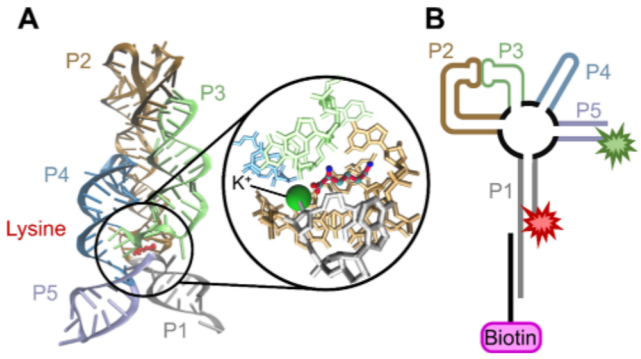

Figure 1. (A) *B. subtilis* lysine riboswitch crystal structure (PDB ID: 3D0U). (B) Biotinylated three-strand RNA construct modified to include FRET pair.

$$\text{Unfolded} + \text{Lysine (U + L)} \rightleftharpoons \text{Unfolded·Lysine (UL)} \rightleftharpoons \text{Folded·Lysine (FL)}$$

Such studies have also found that the lysine dissociation constant (K_D = 0.25 mM) is on the same order as intracellular levels of lysine (10^{-2}−10^{-4} M), which may indicate that the riboswitch is actually thermodynamically rather than kinetically controlled.[44] As one clear corollary, the equilibrium between bound and unbound lysine riboswitch states must be established quickly compared to the subsequent folding dynamics, which can be used to simplify the kinetic analysis.[46]

As the primary focus of this work, temperature-dependent investigations into binding/folding in the lysine riboswitch are pursued using single-molecule wide-field total internal reflection fluorescence (TIRF) microscopy. Specifically, we explore the binding/unbinding and folding/unfolding thermodynamics and kinetics by probing both equilibrium (K_{eq}) and rate (k_{fold}, k_{unfold}) constants over a wide (T = 20−40 °C) temperature range and as a function of lysine concentration (0−4 mM). The temperature-dependent rate and equilibrium constant data are used to construct van't Hoff plots and extract thermodynamic parameters (ΔH, ΔS, ΔG) for the unfolded (U), folded (F), and transition (‡) states. This allows us to obtain free energy, enthalpy, and entropy landscapes for the folding process that elucidate lysine recognition in the binding pocket and how this can affect riboswitch folding and thus gene regulation. Finally, we investigate these energetic landscapes as a function of lysine concentration to interpret the origin of lysine-induced stabilization for the folded state.

II. EXPERIMENTAL SECTION

The crystal structure[47] represented in Figure 1A displays the lysine-bound riboswitch aptamer domain (in red). Upon lysine binding, conformational changes occur with a significant rearrangement in P1 and P5 helices as they move closer together to encapsulate the ligand. With this in mind, we have developed a three-strand construct, with (i) a complementary RNA strand doubly labeled (Cy3-Cy5 FRET pair) on the 5′, 3′ ends (ii) that hybridizes to the terminal P1 and P5 stems to achieve maximize FRET response when in the fully folded conformation and (iii) with a third complementary RNA strand biotinylated at the 3′ end to permit surface tethering necessary for the study of single-molecule kinetics. The three RNA strands are then annealed together and tethered to the

https://doi.org/10.1021/acs.jpcb.1c07833
J. Phys. Chem. B XXXX, XXX, XXX−XXX

surface (see below) to typically achieve surface densities of 0.125 #/μm^2 or ~50 molecules in a 20 × 20 μm^2 field of view. Wide-field laser illumination and detection on a CCD camera are then used to observe time-dependent changes in the single-molecule E_{FRET} value to determine rate (k_{fold}, k_{unfold}) and equilibrium (K_{eq}) constants of the riboswitch as a function of temperature and lysine conditions.

Samples are prepared as previously described[44,48−50] in sandwich-style glass chambers by sequentially flowing solutions of (i) biotinylated bovine serum albumin (BSA), (ii) streptavidin, (iii) the RNA construct, and (iv) an oxygen scavenging cocktail. The biotinylated BSA (10% biotinylated BSA/90% unbiotinylated BSA) coats the glass coverslip surface and binds streptavidin (0.2 mg/mL), which, in turn, binds to and tethers the biotinylated riboswitch. The imaging cocktail contains 50 mM K^+, 100 mM total Na^+, and 0.5 mM Mg^{2+} as background cations, an oxygen scavenging system[51] (TROLOX/PCD/PCA), and lysine to achieve the desired conditions. Each of these three solutions is allowed to incubate for 10 min before the next aliquot flows into the sample chamber. Finally, the sandwich coverslip chamber is sealed with water-resistant glue to eliminate time-dependent drifts due to sample evaporation during data collection.

Although many of our previous kinetics studies exploit the improved time resolution afforded by confocal microscopy,[52] the lysine riboswitch folding/unfolding kinetics are slow enough to permit the use of wide-field TIRF microscopy,[49] which allows simultaneous high-throughput data collection from 10s to 100s of single molecules. As depicted in Figure 2,

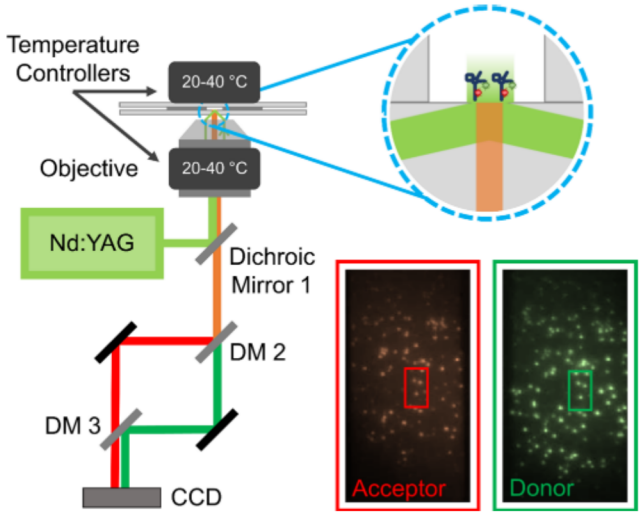

Figure 2. Diagram of TIRF microscope and CCD system with TEC temperature control. The inset shows a cartoon of lysine riboswitch molecules tethered to the glass coverslip. CCD output with offset acceptor and donor channels shows simultaneous data collection of 10s of RNA molecules.

the beam from a 532 nm diode-pumped solid-state laser is sent through a 1.4 NA oil-immersion microscope objective with an appropriately small angle of incidence with the sample surface to achieve total internal reflection.[48] The sample is then illuminated by an evanescent field traveling in solution and parallel to the coverslip, with the resulting fluorescence collected back through the microscope objective. A set of 645 nm long-pass (LP) dichroic mirrors split and recombine the emission is sorted by photon color, with fluorescence from Cy3 (donor) and Cy5 (acceptor) displaced laterally on the CCD camera. The sample data are then collected as a movie and analyzed on LabWindows/CVI software, with correlated pixels from the donor and acceptor fluorescence channels used to construct single-molecule intensity trajectories. Temperature control is achieved by placing a pair of thermoelectric coolers (TECs)[49,52] on top of the sample stage and around the objective. Each of these TECs has a working dynamic range between −20 and 100 °C, i.e., which is more than satisfactory for regulation over the 20−40 °C range of temperatures actually investigated.

III. RESULTS AND ANALYSIS

In the presence of the cognate ligand, riboswitches are capable of the sensitive regulation of gene expression, with the biocompetent folding influenced by cation environment, ligand accessibility, and/or affinity to the binding pocket.[53,54] The overall free energy for its folding event can be usefully deconstructed into enthalpic and entropic landscapes, which reveal valuable insights into how the various folded/unfolded and ligand-bound/unbound conformations (i.e., U + L, UL, and FL) are stabilized and therefore how first folding steps in riboswitch regulation are initiated. In this section, we study lysine concentration-dependent effects on the folding kinetics at both room temperature and over a T = 20−40 °C temperature range through temperature-dependent smFRET. First, lysine-dependent studies at constant temperature are examined in detail in Section III.I and provide further support for an induced-fit (IF) kinetic model for riboswitch folding. This is followed by a discussion of the T-dependent studies in Sections III.II and III.III, which reveal achieving both the transition state ($\Delta H^{\ddagger} < 0$) and fully folded state ($\Delta H^0 < 0$) to be exothermic processes, with a decrease in the entropic cost of riboswitch folding increasing with lysine ligand concentration. Finally, we show that these lysine-dependent entropic effects occur primarily in the folding mechanism, with relatively minor influence on the corresponding unfolding pathway.

III.I. Lysine Riboswitch Folds via an Induced-Fit (IF) Pathway. To extract kinetic rate constants for folding/unfolding, we analyze emission intensity trajectory data for each RNA molecule (Figure 3A) by first converting count rates into E_{FRET} values via $E_{FRET} = I_A/(I_A + I_D)$. These E_{FRET} trajectories reveal two well-resolved FRET states ($E_{FRET} \approx$ 0.4 and 0.8), with low and high FRET values corresponding to unfolded and folded conformations of the riboswitch, respectively. To establish dwell time distributions for each folded and unfolded state event, the FRET threshold value is selected as the local histogramic minimum (dashed line in Figure 3A, lower panel) between high and low FRET states. These dwell times are then compiled into a cumulative distribution function (CDF; Figure 3B),[55] which reflects survival probabilities as a function of the unfolded or folded event durations. The CDF data in Figure 3B can be well fit by single-exponential decay to yield k_{fold} and k_{unfold} rate constants, consistent with a kinetic treatment of folding and unfolding as elementary processes. The equilibrium constant K_{eq} is computed from the ratio of total times ($t_{folded}/t_{unfolded}$) that the riboswitch spends in the folded vs unfolded states, though it may equivalently be obtained from (and indeed agrees with) ratios of the measured rate constants (k_{fold}/k_{unfold}). Reported errors are calculated as the standard deviation of the mean from three data sets, with standard errors shown in parentheses (e.g., 0.545(5) = 0.545 ± 0.005).

https://doi.org/10.1021/acs.jpcb.1c07833
J. Phys. Chem. B XXXX, XXX, XXX−XXX

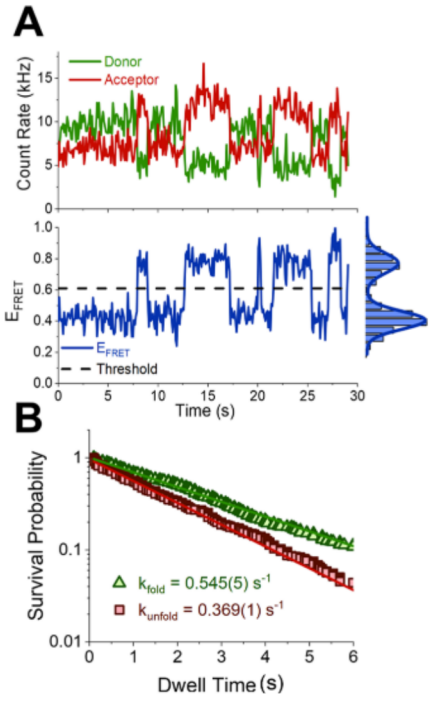

Figure 3. Single-molecule sample data. (A) Donor (green) and acceptor (red) channel intensity trajectories and corresponding E_{FRET} (blue) trajectory and histogram. The threshold value between folded and unfolded states is found between E_{FRET} peaks. (B) Survival probability of folded (red squares) and unfolded (green triangles) dwell times fit to single exponentials to find k_{unfold} and k_{fold}, respectively.

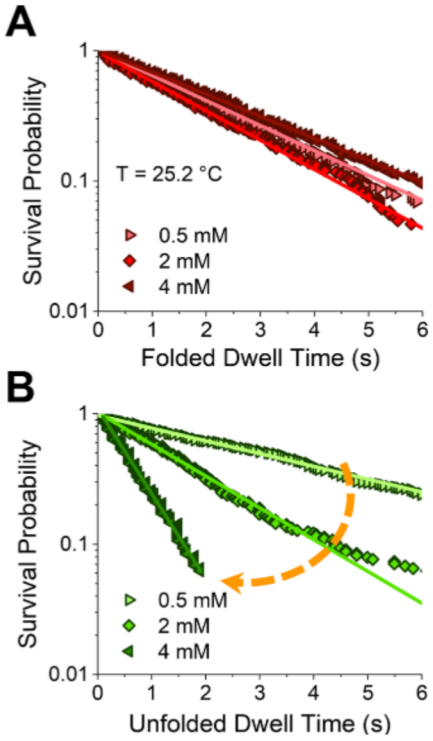

Figure 4. Lysine concentration effects on rate constants. Data point and fit colors are light to dark with increasing lysine concentration. (A) Folded state survival probabilities show lysine independence in k_{unfold}. (B) Unfolded state survival probabilities show increasing k_{fold} with increasing lysine concentration.

Figure 4 illustrates the lysine dependence on the riboswitch rate constants. Notably, the folding rate constant for the riboswitch increases dramatically with lysine concentration (Figure 4B), while the unfolding rate constant remains essentially lysine-independent (Figure 4A). This lack of ligand dependence in k_{unfold} is consistent with riboswitch unfolding as a unimolecular kinetic process [i.e., folded (F) ⇌ unfolded (U)]. Conversely, folding must include a lysine-dependent step, such as lysine binding, to elicit a FRET response. These results, tabulated in SI, are consistent with previous reports[33,44] of a three-state induced-fit folding kinetic pathway, specifically the existence of an unfolded lysine-unbound (U + L) state, an unfolded lysine-bound state (UL), and a folded lysine-bound state (FL)

$$\mathrm{U} + \mathrm{L} \overset{K_L}{\rightleftharpoons} \mathrm{UL} \underset{k_{-1}}{\overset{k_1}{\rightleftharpoons}} \mathrm{FL}$$

where K_L is the lysine dissociation constant and k_1 and k_{-1} are the elementary rate constants. In such a model, both the U + L and UL states are assumed to have equivalent low FRET values, as the P1 and P5 helices have not yet closed around the ligand, with the high FRET value representing the ligand-bound FL state. In agreement with this simple three-state model, therefore, folding of the riboswitch would feature lysine-dependent kinetics

$$\mathrm{U} + \mathrm{L} \overset{K_L}{\rightleftharpoons} \mathrm{UL} \overset{k_1}{\rightarrow} \mathrm{FL},\ k_{fold} = \frac{k_1[\mathrm{L}]}{[\mathrm{L}] + K_L}$$

whereas unfolding is correctly predicted to be independent of ligand

$$\mathrm{FL} \underset{k_{-1}}{\longrightarrow} \mathrm{UL},\ k_{unfold} = k_{-1}$$

It is briefly worth contrasting this with predictions for a corresponding conformational selection (CS) kinetic model

$$\mathrm{U} + \mathrm{L} \underset{k_{-1}}{\overset{k_1}{\rightleftharpoons}} \mathrm{F} + \mathrm{L} \overset{K_L}{\rightleftharpoons} \mathrm{FL}$$

which requires folding of the riboswitch *prior to* ligand binding. Low FRET values would therefore correspond to the unfolded/ligand-unbound state (U), with the folded/ligand-unbound (F) and folded/ligand-bound states (FL) exhibiting comparably high FRET values. In such an alternate CS kinetic scenario, one would predict the effective folding rate constant (k_{fold}) to be independent of lysine, with a decrease in both [FL] and effective unfolding rate constant (k_{unfold}) with increasing lysine. As the experimental data clearly demonstrate a strong ligand-dependent k_{fold} with essentially no corresponding ligand dependence for k_{unfold}, this rationalizes utilizing an induced-fit (IF) kinetic model (as anticipated) to interpret the lysine riboswitch folding dynamics.

III.II. Access to the Folding Transition State Is Exothermically Favored with Entropic Penalty. In addition to the above kinetic studies at a fixed temperature, even more information becomes available from *T*-dependent studies. Specifically, kinetic analysis over a range of temperatures ($T \approx 20$–40 °C) yields folding thermodynamics as characterized by the equilibrium van't Hoff expressions

https://doi.org/10.1021/acs.jpcb.1c07833
J. Phys. Chem. B XXXX, XXX, XXX−XXX

$$K_{eq} = \exp(-\Delta G^{\circ}/RT)$$

$$\ln(K_{eq}) = -(\Delta H^{\circ}/R)(1/T) + \Delta S^{\circ}/R$$

which allow us to deconstruct the overall free-energy change into enthalpic and entropic components,[52,56,57] assuming that the standard enthalpy/entropy changes are constant under the temperature range. This can be taken one step further by temperature-dependent analysis of the rate constants, which from transition-state theory (TST) provides equivalent information on thermodynamics of the rate-limiting transition state[32,52,58]

$$\ln(k_{fold(unfold)}) = (-\Delta G^{\ddagger})/RT - \ln(\kappa\upsilon)$$

where υ represents the unimolecular attempt frequency for folding or unfolding and κ is the transmission coefficient. By way of example, Figure 5 reveals sample data on temperature-dependent riboswitch folding and unfolding at a constant lysine concentration (2 mM). Both rate constants are clearly strongly affected by temperature, but in opposite directions, with k_{fold} decreasing and k_{unfold} increasing with increasing T. Such data unambiguously indicate the net experimental decrease in equilibrium constant K_{eq}, with T clearly arising from both T-dependent stabilization and destabilization of the unfolded and folded states, respectively (see the Supporting Information, SI for quantitative data).

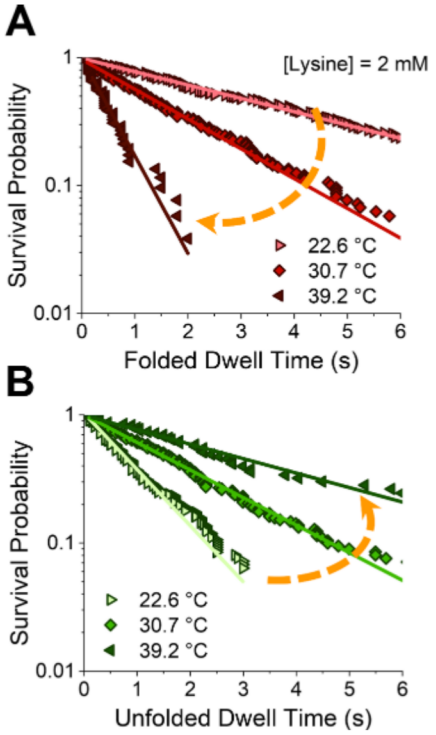

Figure 5. Temperature dependence of rate constants for the riboswitch folding reaction at 2 mM lysine. (A) Increasing temperature increases k_{unfold} and (B) decreases k_{fold}.

To extract enthalpic and entropic contributions associated with such a conformational change, we have investigated the equilibrium constant for riboswitch folding over 20−40 °C, with van't Hoff analysis summarized in a $\log(K_{eq})$ vs $1/T$ plot in Figure 6A. The slope of the data for the folding process (U → F) is strongly positive and thus overall exothermic, with a

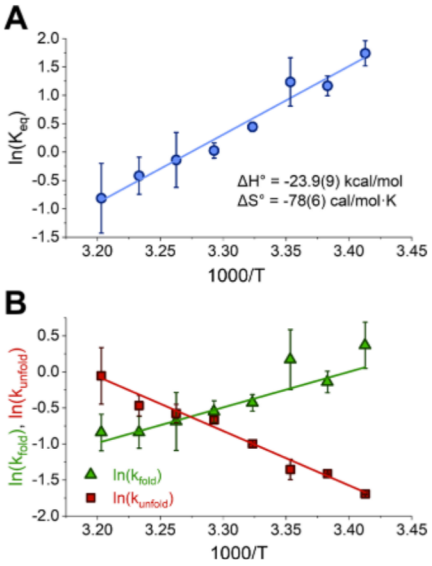

Figure 6. van't Hoff analysis of the riboswitch at 2 mM lysine. (A) K_{eq} temperature dependence to find the standard enthalpy and standard entropy of folding $\ln(K_{eq}) = -(\Delta H^{\circ}/R)(1/T) + \Delta S^{\circ}/R$. Folding is exothermic (positive slope) and entropically costly (negative intercept). (B) k_{fold} (green triangles) and k_{unfold} (red squares) temperature dependences to find transition-state enthalpy and entropy $\ln(k_{fold}) = (-\Delta G^{\ddagger})/RT - \ln(\kappa\upsilon)$. Positive slope in k_{fold} and negative slope in k_{unfold} indicate that the transition state is enthalpically downhill from the unfolded state.

standard enthalpy change of $\Delta H^{\circ} = -23.9(9)$ kcal/mol, which can be attributed to the formation of 6−7 hydrogen bonds between the lysine ligand and internal contacts on the riboswitch,[8] though various other interactions between water molecules, solvated ions, lysine, and the riboswitch may also be at play. Furthermore, the negative intercept signals that the riboswitch conformation becomes restricted and/or the lysine more tightly constrained, contributing to a significant decrease in the entropy of $\Delta S^{\circ} = -78(6)$ cal/(mol·K) for the forward (U → F) reaction.

These overall enthalpic and entropic contributions can be further broken down into the unfolded to transition state (U → ‡) and transition state to folded (‡ → F) components, which can be determined via the transition-state theory temperature analysis[25,35] of the corresponding rate constants

$$\ln(k_{fold(unfold)}) = -(\Delta H^{\ddagger}_{fold(unfold)} - T\Delta S^{\ddagger}_{fold(unfold)})/RT + \ln(\kappa\upsilon_{fold(unfold)})$$

Similar to van't Hoff analysis, the transition-state enthalpy and entropy changes are encoded in the slopes and intercepts ($m = -\Delta H^{\ddagger}$, $b = \Delta S^{\ddagger}/R - \ln(\kappa\upsilon)$) in Figure 6B, which immediately indicate that kinetic access to the folding (unfolding) transition state releases (absorbs) heat. Establishing the absolute entropy for the transition state is less straightforward because the attempt frequencies ($\kappa\upsilon$) are not known *a priori*, though the intercepts are only logarithmically dependent on this assumed value ($\kappa\upsilon \approx 10^6$ s^{-1}).[59] Nevertheless, the negative intercept in Figure 6B already reveals $-T\Delta S^{\ddagger} > 0$ to be a predominant contribution to the transition-state barrier free energy for folding, which, in turn, tightly controls folding/unfolding kinetic rates. It is worth noting that despite a potential ambiguity in absolute entropy values, differential changes in

https://doi.org/10.1021/acs.jpcb.1c07833
J. Phys. Chem. B XXXX, XXX, XXX−XXX

the TS entropy ($\Delta\Delta S^{\ddagger}$) are completely independent of κv. Thus, any lysine-dependent entropic effects ($\Delta(-T\Delta S^{\ddagger})$) on the transition-state barrier can be rigorously extracted, as discussed below.

The thermodynamic quantities are summarized in Figure 7 to depict enthalpic and entropic landscapes along the folding/unfolding coordinate. First of all, the enthalpy change between the folded and transition-state conformations is strongly exothermic ($\Delta H^{\ddagger} < 0$) but represents only 45% of the overall ΔH^0, suggesting a similar fraction of the bonding interactions (i.e., ~2−3 hydrogen bonds) between lysine and the riboswitch at the transition state. Conversely, the entropy change in accessing the transition state ($\Delta S^{\ddagger}$) is strongly negative but now within 10% of the overall ΔS^0, which is consistent with most of the structural rearrangement and solvent reorganization occurring by the transition state. In the context of an induced-fit model, lysine must first bind to the riboswitch before it can fold. However, as $|\Delta H^{\ddagger}| < |\Delta H^0|$ and $\Delta S^{\ddagger} \approx \Delta S^0$, only some subset (≤45%) of the bonding between lysine and the riboswitch is needed to trigger folding. The UL state should therefore occur before the transition state and be enthalpically favorable with respect to reactants (U + L) but not as favorable as the transition state. As a visual guide, we indicate the approximate enthalpy of UL in Figure 7A, though an exact value is indeterminate from the data.

If we combine these entropic and enthalpic contributions, one predicts a transition-state free-energy barrier of $\Delta G^{\ddagger}$ = +8(5) kcal/mol, dominated by the entropic confinement of the lysine-bound riboswitch, as well as changes in water and ion content. As a result, enthalpically favorable ($\Delta H_{fold}{}^{\ddagger}$ = −10(2) kcal/mol) bond formation takes place only after folding into the correct conformational shape is largely achieved (with an entropic penalty of $\Delta S_{fold}{}^{\ddagger}$ = −61(9) cal/(mol·K)). This constitutes a classic example of compensating entropic vs enthalpic contributions at 300 K, resulting in a strongly rate-limited free-energy kinetic barrier and yet only a modest (ΔG^0 = −0.5 ± 3 kcal/mol) overall free-energy change for folding.

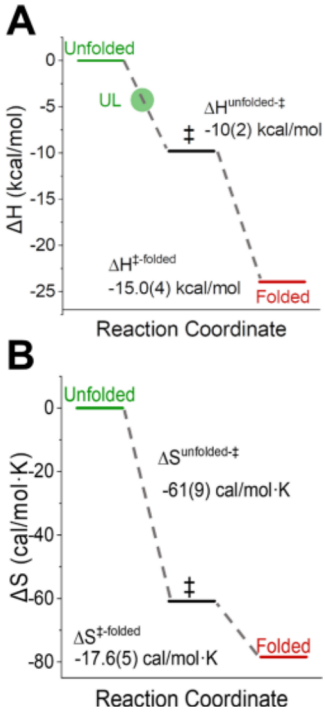

Figure 7. (A) Enthalpy landscape of the folding reaction. The lysine-bound unfolded state (UL) and transition state (‡) lie between the unfolded and folded states. Exact placement of UL in this plot is underdetermined, but it is very likely between the reactants and the transition state in enthalpy. (B) Entropy landscape of the folding reaction shows a large entropic cost in reaching the transition state and a subsequent penalty to proceed further to the folded state.

III.III. Lysine-Promoted Folding Is an Entropic Effect. We next consider the impact of lysine ligand on the riboswitch folding thermodynamics, which has been explored over a wide range of concentrations (100 μM to 4 mM) and temperatures (20−40 °C), with results presented as an overlapping series of composite van't Hoff plots in Figure 8. At each lysine concentration, the van't Hoff plots systematically reveal large overall exothermicities (positive slopes, $\Delta H^0 < 0$) and yet with a strong compensatory decrease in entropies (negative intercepts, $\Delta S^0 < 0$) upon folding. Simply summarized, there is a systematic parallel shift upward in the van't Hoff plot structure due to a lysine-induced increase in entropic stability for the folded conformation. This is of course consistent with the previous kinetic data at room temperature (Figure 4), which predicts a systematic increase in K_{eq} with lysine arising predominantly from a lysine-dependent increase in k_{fold} at nearly constant k_{unfold}.

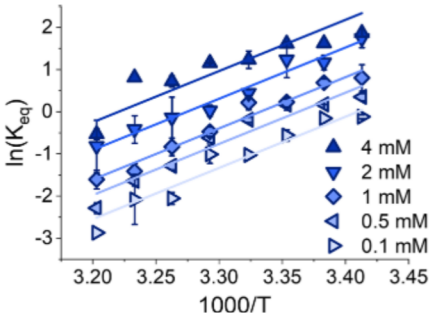

Figure 8. van't Hoff analysis of the riboswitch at different lysine concentrations. The overall trend indicates that lysine stabilizes the folded state ($\Delta K_{eq} > 0$), likely due to entropic rather than enthalpic effects (similar slopes, changing intercepts).

The key point of interest is whether such a lysine-dependent increase in riboswitch stability arises from (i) more favorable enthalpic heat release ($\Delta\Delta H^0 < 0$) or (ii) a decrease in entropic penalty ($\Delta\Delta S^0 > 0$) with increasing lysine. A predominance of entropic effects in the lysine dependence of K_{eq} could simply reflect ligand acceleration of the binding process (U + L → UL) and therefore folding. This is effectively an increase in the population of microstates that allow lysine to access the riboswitch binding site, which would diminish the corresponding entropic cost to binding. If so, one would predict a series of parallel plots in Figure 8 with corresponding increases in the intercepts. Indeed, the quantitative inspection of Figure 8 reveals each linear van't Hoff plot to be systematically shifted upward ($\Delta\Delta S^0 > 0$) yet maintaining a comparable slope ($\Delta\Delta H^0 \approx 0$). This bolsters the argument that the experimentally observed increase in K_{eq} occurs not by enthalpic gain but rather by decrease in entropic cost ($\Delta\Delta S^0 > 0$) for folding at higher ligand concentration.

Conversely, any lysine-dependent enthalpic change must arise in the binding equilibrium step, U + L ⇌ UL, where increased lysine concentration shifts the equilibrium such that

https://doi.org/10.1021/acs.jpcb.1c07833
J. Phys. Chem. B XXXX, XXX, XXX−XXX

the initial unfolded state (U) more closely resembles the UL state than U + L. Thus, if the fractional change in ΔH between U + L and UL is large, this would translate into correspondingly large changes in ΔH^0 as a function of different lysine concentrations ($\Delta H^0_{0.1\text{ mM lys}} \neq \Delta H^0_{4\text{ mM lys}}$). For ΔH^0 to remain constant, therefore ($\Delta H^0_{0.1\text{ mM lys}} \approx \Delta H^0_{4\text{ mM lys}}$), ΔH must be very small, consistent with the UL state exhibiting only a small number of hydrogen bonds between lysine and the riboswitch. This is possible, as the combination of a large entropic barrier ($-T\Delta S^{\ddagger} \approx -T\Delta S^0 > 0$) with comparatively smaller enthalpic contributions indicates that the riboswitch is mostly folded by the transition state but that the hydrogen bond formation is largely incomplete. Such a line of argument would suggest any differential enthalpic shifts between U + L ⇌ UL to be small, and any changes in this equilibrium due to lysine concentration would not significantly affect our assumption of $\Delta\Delta H^0 \approx 0$, as indeed confirmed by experiment.

IV. DISCUSSION

IV.I. Riboswitch Binding Pocket Structure Provides Enthalpic and Entropic Contributions to the Folding Free-Energy Landscape. The lysine riboswitch exhibits high specificity for its cognate ligand over similar species such as *S*-(2-aminoethyl)-L-cysteine, L-4-oxalysine, or L-homoarginine, so much so that it requires 10−100× higher concentrations of these analogues than lysine to achieve gene regulation in *in vitro* biochemical assays.[11] This highlights the importance of multiple contact points between the binding pocket and all moieties of lysine, specifically the carboxyl, the α-amino, and the main-chain lysyl groups, as shown in Figure 1A. The carboxylate group has a potassium-mediated interaction with a guanine group in the RNA as well as direct hydrogen bonding with two other guanine groups, the α-amino group bonds with one of these guanine groups, and the lysyl group bonds with still another guanine group, a cytosine group, and an ordered water molecule.[1,11] The overall exothermicity ($\Delta H^\circ = -25(2)$ kcal/mol) experimentally measured and visually represented in Figure 7A corroborates the numerous interactions as a result of lysine recognition by the aptamer domain, those that involve direct lysine riboswitch binding as well as subsequent indirect contributions between the folded riboswitch, ions, and water molecules in solution. The weaker but still significantly exothermic nature of the approach to folding ($\Delta H^{\ddagger} = -10(2)$ kcal/mol) speaks again to the partial (≈45%) formation of these lysine riboswitch and riboswitch−ion interactions already by the transition state.

The system experiences several changes in RNA conformation as well as changes in ordered solvent and cation content during binding and folding. These changes certainly include the P1−P5 closure and lysine orientation within the binding pocket but may also involve the ordering of cation or water content as the riboswitch expels water upon folding,[26] with some remaining water bound to either lysine, the potassium ion, or bridging between the ligand and the riboswitch.[11] Interestingly, the major entropic cost in the reaction is predominantly between the unfolded and transition states, with $\Delta S_{(\text{fold})}^{\ddagger} = -61(9)$ cal/(mol·K), ∼80% of the overall $\Delta S^\circ = -78(6)$ kcal/mol. This indicates that although only some ($n \approx 3$) of the total H-bonds ($n_{\text{tot}} \approx 6-7$) involved in the overall folding are formed between the unfolded and transition states, this is evidently sufficient to induce structural rearrangement characteristic of the low entropy folded state with bound lysine.

IV.II. Lysine Decreases the Entropic Transition-State Barrier to Folding. To further understand the entropic benefit of higher ligand concentration on riboswitch folding, we have examined lysine-induced changes to the transition state by studying its effects on k_{fold} and k_{unfold}. The data in Figure 9 show strong lysine-dependent impacts on the folding rates but almost negligible variation in the unfolding rate constants. It is worth noting that the highest temperature data at [lysine] = 0.1 mM deviate somewhat from the trend, which we attribute mainly to the difficulty in collecting data under unstable equilibrium constant conditions ($K_{\text{eq}} < 0.1$). Otherwise, the trend is of course consistent with room-temperature kinetic studies (e.g., Figure 4) that recapitulate a lysine-independent k_{unfold} and yet a lysine-induced increase in k_{fold}. Similar to T-dependent van't Hoff behavior in K_{eq} (see Figure 8), the main lysine effect on k_{fold} appears to be slope-conserving vertical shifts (i.e., nearly purely entropic), though obtaining accurate $\Delta\Delta S^{\ddagger}$ information can be difficult due to $\Delta H^{\ddagger}$ and $\Delta S^{\ddagger}$ parameter correlations. However, as similarly argued in Section III.III, the data are consistent with an approximately constant folding transition-state enthalpy, independent of lysine concentration ($\Delta\Delta H_{\text{fold}}^{\ddagger} \approx 0$). Consequently, the transition-state theory Eyring plots in Figure 9 have been least-squares fit globally with a common slope (i.e., $\Delta H^{\ddagger} = -11(1)$ kcal/mol, summarized in SI) to break this correlation and better estimate the corresponding entropies.

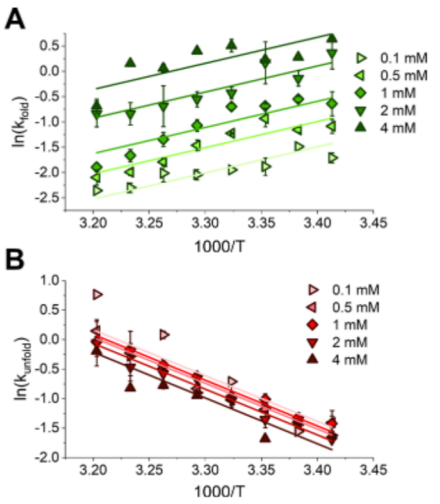

Figure 9. Lysine concentration effects on folding and unfolding rate constants. (A) k_{fold} dramatically increases with lysine concentration, which indicates a decreased energetic barrier to the transition state. (B) k_{unfold}, and therefore the energy barrier between the folded and transition states, is mostly independent of lysine concentration.

The resulting entropic ($-T\Delta S$) and free-energy (ΔG) contributions from such fits are visually summarized in Figure 10 and represent the lysine-dependent free-energy landscape for riboswitch folding. The corresponding $-T\Delta S$ (Figure 10A) and ΔG (Figure 10B) values are calculated at $T = 300$ K; these are plotted for each lysine concentration as a function of reaction coordinate, all referenced to the unfolded and unbound riboswitch state at 0 kcal/mol. The free-energy landscape clearly shows that riboswitch folding shifts between thermodynamically favorable and unfavorable over a relatively modest range of lysine concentrations. It is important to note,

https://doi.org/10.1021/acs.jpcb.1c07833
J. Phys. Chem. B XXXX, XXX, XXX−XXX

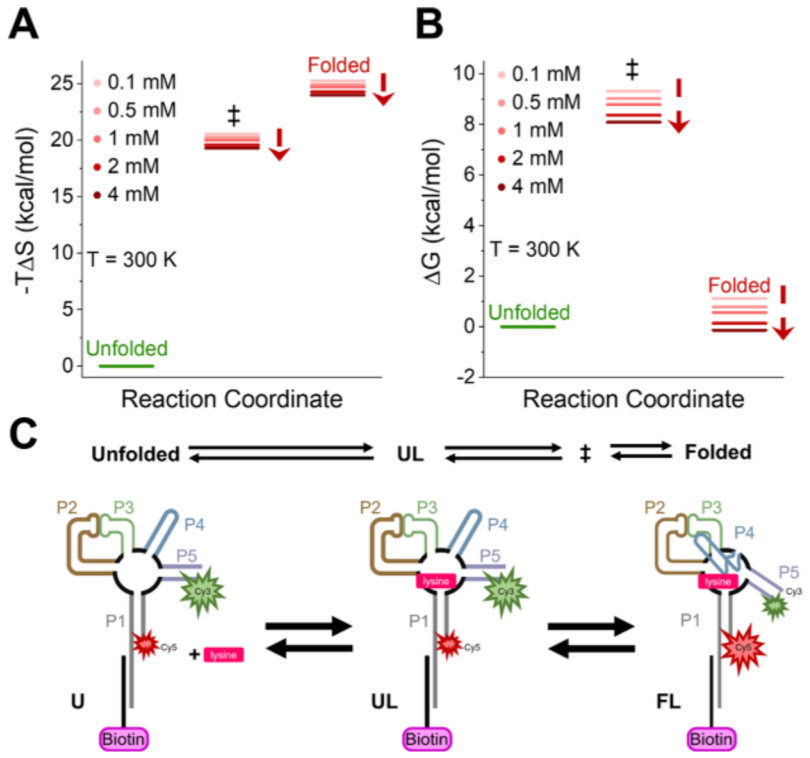

Figure 10. Energetic landscape of the riboswitch folding reaction at different lysine concentrations. Changes in entropy and free energy are referenced to the unfolded state at 0 kcal/mol. (A) The entropic component of the reaction's free energy shows a decreased entropic cost to the transition-state barrier and the folded state. (B) The free-energy landscape shows that the unfolded ⇌ folded reaction can be exergonic or endergonic depending on the lysine concentration. The transition-state barrier, and consequently folding kinetics, is dictated by the entropic cost of reaching the transition state. Panel (C) depicts the U + L, UL, and FL states with a comparison to the reaction coordinate timeline.

however, that there is always a rate-determining transition-state barrier to folding/unfolding at all lysine values, small changes which serve to regulate the folding/unfolding rate constants. As demonstrated in Figures 8 and 9, the thermodynamic origin of this barrier to folding is largely entropic, yet dramatically controls the reaction kinetics and dwell times for the riboswitch in folded and unfolded states. Conversely, the entropic contributions to free energies of the transition and folded states vary with lysine at almost identical rates. Thus, the $-T\Delta S^{\ddagger}$ contribution to the folding free-energy barrier decreases dramatically with increasing lysine concentration, whereas there is little change in the corresponding free-energy barrier to unfolding. It is this entropic, lysine-dependent control of forward (reverse) free-energy barriers that is the fundamental thermodynamic reason behind the strong (weak) lysine-dependent promotion of riboswitch folding (unfolding) rate constants, respectively. Finally, states along the reaction coordinate are denoted alongside the states in the induced-fit riboswitch folding mechanism (Figure 10C). This new, simultaneous comparison of information from concentration and temperature-dependent data can be used to develop a physical picture for the transition state, in which lysine is loosely bound through specific contacts in the binding pocket and the riboswitch has mostly folded around it.

Lysine is present only in 100-fold smaller concentrations than background cations (e.g., a few mM vs 150 mM K^+ and Na^+). It is therefore unlikely that such entropic effects derive primarily from solvent and solution ion ordering around bare lysine in the unbound riboswitch conformation. Instead, it is more plausible that this entropy reduction arises from the lysine recognition of different functional groups by specific points of contact in the riboswitch binding pocket. For this putative "bind-then-fold" (IF) mechanism, the initial lysine binding step is necessarily bimolecular, meaning that increased ligand concentrations enhance K_{eq} by increasing the pseudo-zeroth-order unimolecular rate constant for folding (k_{fold}). As a simple kinetic picture, increased ligand naturally results in higher concentrations of lysine correctly oriented with respect to the aptamer binding domain, thereby satisfying the requirements for low entropy and thereby reducing $-T\Delta S^{\ddagger}$ entropic contributions to the free-energy barrier for riboswitch folding.

V. CONCLUSIONS

Temperature-dependent equilibrium and kinetic studies of the lysine riboswitch have been performed at the single-molecule level, permitting detailed thermodynamic deconstruction of entropic and enthalpic contributions to the free-energy folding pathway. In agreement with previous studies, we find that riboswitch stability (K_{eq}) and folding rate constant (k_{fold}) are dramatically accelerated by increased lysine concentration, with essentially no impact on the corresponding unfolding rates (k_{unfold}). From the Eyring theory analysis of the temperature-dependent kinetic studies, the riboswitch is found to have satisfied most of the entropic cost for folding by the time it reaches the transition state ($\Delta S^{\ddagger} \approx \Delta S^{\circ}$), yet with only a modest fraction of the stabilizing interactions having been formed ($\Delta H^{\ddagger} \approx 45\%$ of ΔH°). This competition between entropy and enthalpy at the transition state results in a larger free-energy barrier ($\Delta G^{\ddagger} = +8(2)$ kcal/mol at 2 mM lysine and 300 K) that strongly regulates folding kinetics before reaching the final folded state, despite only a small

https://doi.org/10.1021/acs.jpcb.1c07833
J. Phys. Chem. B XXXX, XXX, XXX−XXX

change in the overall free energy ($\Delta G^0 = -0.1 \pm 2$ kcal/mol). Finally, increased lysine concentration is shown to entropically regulate the kinetics by lowering entropic costs at the transition-state barrier and thereby dramatically increasing the rate constant for folding.

As a parting comment, we might expect such entropic vs enthalpic thermodynamic control of riboswitch folding to offer differential evolutionary advantages depending on the environmental conditions. Specifically, it would be interesting to quantitatively compare the thermodynamics of lysine riboswitches prevalent in different organisms and to explore evolution in and bioadaptation to different ecosystems. For example, the results reported herein for *Bacillus subtilis*, which prefer mild temperatures (~40 °C), would juxtapose well with parallel studies of riboswitches from hyperthermophilic bacteria, e.g., *Thermotoga maritima*, that thrive in elevated temperature (~80 °C) environments.[47] These thermophilic riboswitches might provide an especially interesting contrast, as the *B. subtilis* lysine riboswitch exhibits strongly exothermic folding, which, by Le Chatelier's principle, would predict lower stability and less efficient regulation ($k_{unfold} \gg k_{fold}$) at the higher temperatures preferred by *T. maritima*. Also of interest would be the effect of mono- and divalent cation conditions on riboswitch folding. Indeed, of particular relevance would be the special role of monovalent K^+, which at least for the *B subtilis* lysine riboswitch appears to be an essential metabolite required at ≈ mM concentrations for biochemically competent folding.[21,44,45] Efforts in both of these directions are currently underway, with the elucidation of such thermodynamic and small cation effects hopefully able to help explain how both mesophilic and thermophilic bacteria are able to succeed in their respective environments.

■ ASSOCIATED CONTENT

Supporting Information

The Supporting Information is available free of charge at https://pubs.acs.org/doi/10.1021/acs.jpcb.1c07833.

Tables of values and uncertainties associated with the data plotted in Figures 4, 5, and 8−10 (PDF)

■ AUTHOR INFORMATION

Corresponding Author

David J. Nesbitt − *JILA, University of Colorado Boulder and National Institute of Standards and Technology, Boulder, Colorado 80309, United States; Department of Chemistry, University of Colorado Boulder, Boulder, Colorado 80309, United States; Department of Physics, University of Colorado Boulder, Boulder, Colorado 80309, United States;* orcid.org/0000-0001-5365-1120; Email: djn@jila.colorado.edu

Author

Andrea Marton Menendez − *JILA, University of Colorado Boulder and National Institute of Standards and Technology, Boulder, Colorado 80309, United States; Department of Chemistry, University of Colorado Boulder, Boulder, Colorado 80309, United States*

Complete contact information is available at: https://pubs.acs.org/10.1021/acs.jpcb.1c07833

Notes

The authors declare no competing financial interest.

■ ACKNOWLEDGMENTS

Initial support for this work was through the National Science Foundation under grant CHE-1665271/2053117 from the Chemical, Structure, Dynamics and Mechanisms-A Program, with recent transitional support from the Air Force Office of Scientific Research (FA9550-15-1-0090) and additional funds for the development of the confocal apparatus from PHY-1734006 (Physics Frontier Center Program). The authors would also like to acknowledge early seed contributions by the W. M. Keck Foundation Initiative in RNA Sciences at the University of Colorado, Boulder.

■ REFERENCES

(1) Smith-Peter, E.; Lamontagne, A. M.; Lafontaine, D. A. Role of Lysine Binding Residues in the Global Folding of the Lysc Riboswitch. *RNA Biol.* **2015**, *12*, 1372−1382.

(2) Croft, M. T.; Moulin, M.; Webb, M. E.; Smith, A. G. Thiamine Biosynthesis in Algae Is Regulated by Riboswitches. *Proc. Natl. Acad. Sci. U.S.A.* **2007**, *104*, 20770−20775.

(3) Mandal, M.; Breaker, R. R. Adenine Riboswitches and Gene Activation by Disruption of a Transcription Terminator. *Nat. Struct. Mol. Biol.* **2004**, *11*, 29−35.

(4) Barrick, J. E.; Corbino, K. A.; Winkler, W. C.; Nahvi, A.; Mandal, M.; Collins, J.; Lee, M.; Roth, A.; Sudarsan, N.; Jona.; et al. New RNA Motifs Suggest an Expanded Scope for Riboswitches in Bacterial Genetic Control. *Proc. Natl. Acad. Sci. U.S.A.* **2004**, *101*, 6421−6426.

(5) Nahvi, A.; Barrick, J. E.; Breaker, R. R. Coenzyme B12 Riboswitches Are Widespread Genetic Control Elements in Prokaryotes. *Nucleic Acids Res.* **2004**, *32*, 143−150.

(6) Mandal, M.; Boese, B.; Barrick, J. E.; Winkler, W. C.; Breaker, R. R. Riboswitches Control Fundamental Biochemical Pathways in *Bacillus subtilis* and Other Bacteria. *Cell* **2003**, *113*, 577−586.

(7) Argaman, L.; Hershberg, R.; Vogel, J.; Bejerano, G.; Wagner, E. G. H.; Margalit, H.; Altuvia, S. Novel Small RNA-Encoding Genes in the Intergenic Regions of Escherichia Coli. *Curr. Biol.* **2001**, *11*, 941−950.

(8) Gilbert, S. D.; Love, C. E.; Edwards, A. L.; Batey, R. T. Mutational Analysis of the Purine Riboswitch Aptamer Domain. *Biochemistry* **2007**, *46*, 13297−13309.

(9) Tucker, B. J.; Breaker, R. R. Riboswitches as Versatile Gene Control Elements. *Curr. Opin. Struct. Biol.* **2005**, *15*, 342−348.

(10) Nguyen, G. T. D. T.; Scaife, M. A.; Helliwell, K. E.; Smith, A. G. Role of Riboswitches in Gene Regulation and Their Potential for Algal Biotechnology. *J. Phycol.* **2016**, *52*, 320−328.

(11) Serganov, A.; Huang, L.; Patel, D. J. Structural Insights into Amino Acid Binding and Gene Control by a Lysine Riboswitch. *Nature* **2008**, *455*, 1263−1267.

(12) Dambach, M.; Sandoval, M.; Updegrove, T. B.; Anantharaman, V.; Aravind, L.; Waters, L. S.; Storz, G. The Ubiquitous Ybp-Ykoy Riboswitch Is a Manganese-Responsive Regulatory Element. *Mol. Cell* **2015**, *57*, 1099−1109.

(13) Ren, A.; Rajashankar, K. R.; Patel, D. J. Fluoride Ion Encapsulation by Mg^{2+} Ions and Phosphates in a Fluoride Riboswitch. *Nature* **2012**, *486*, 85−89.

(14) Hallberg, Z. F.; Su, Y.; Kitto, R. Z.; Hammond, M. C. Engineering and in Vivo Applications of Riboswitches. *Annu. Rev. Biochem.* **2017**, *86*, 515−539.

(15) Montange, R. K.; Mondragón, E.; van Tyne, D.; Garst, A. D.; Ceres, P.; Batey, R. T. Discrimination between Closely Related Cellular Metabolites by the Sam-I Riboswitch. *J. Mol. Biol.* **2010**, *396*, 761−772.

(16) Gilbert, S. D.; Reyes, F. E.; Edwards, A. L.; Batey, R. T. Adaptive Ligand Binding by the Purine Riboswitch in the Recognition of Guanine and Adenine Analogs. *Structure* **2009**, *17*, 857−868.

(17) Polaski, J. T.; Webster, S. M.; Johnson, J. E.; Batey, R. T. Cobalamin Riboswitches Exhibit a Broad Range of Ability to

Discriminate between Methylcobalamin and Adenosylcobalamin. *J. Biol. Chem.* **2017**, *292*, 11650−11658.
(18) Chen, L.; Cressina, E.; Dixon, N.; Erixon, K.; Agyei-Owusu, K.; Micklefield, J.; Smith, A. G.; Abell, C.; Leeper, F. J. Probing Riboswitch-Ligand Interactions Using Thiamine Pyrophosphate Analogues. *Org. Biomol. Chem.* **2012**, *10*, 5924−5931.
(19) Edwards, A. L.; Reyes, F. E.; Héroux, A.; Batey, R. T. Structural Basis for Recognition of S-Adenosylhomocysteine by Riboswitches. *RNA* **2010**, *16*, 2144−2155.
(20) Garst, A. D.; Porter, E. B.; Batey, R. T. Insights into the Regulatory Landscape of the Lysine Riboswitch. *J. Mol. Biol.* **2012**, *423*, 17−33.
(21) Garst, A. D.; Edwards, A. L.; Batey, R. T. Riboswitches: Structures and Mechanisms. *Cold Spring Harbor Perspect. Biol.* **2011**, *3*, No. a003533.
(22) Harbaugh, S. V.; Martin, J. A.; Weinstein, J.; Ingram, G.; Kelley-Loughnane, N. Screening and Selection of Artificial Riboswitches. *Methods* **2018**, *143*, 77−89.
(23) Ellington, A. D.; Szostak, J. W. In Vitro Selection of RNA Molecules That Bind Specific Ligands. *Nature* **1990**, *346*, 818−822.
(24) Chi, C. W.; Lao, Y. H.; Li, Y. S.; Chen, L. C. A Quantum Dot-Aptamer Beacon Using a DNA Intercalating Dye as the FRET Reporter: Application to Label-Free Thrombin Detection. *Biosens. Bioelectron.* **2011**, *26*, 3346−3352.
(25) Jo, H.; Ban, C. Aptamer−Nanoparticle Complexes as Powerful Diagnostic and Therapeutic Tools. *Exp. Mol. Med.* **2016**, *48*, No. e230.
(26) Blount, K. F.; Breaker, R. R. Riboswitches as Antibacterial Drug Targets. *Nat. Biotechnol.* **2006**, *24*, 1558−1564.
(27) Sudarsan, N.; Cohen-Chalamish, S.; Nakamura, S.; Emilsson, G. M.; Breaker, R. R. Thiamine Pyrophosphate Riboswitches Are Targets for the Antimicrobial Compound Pyrithiamine. *Chem. Biol.* **2005**, *12*, 1325−1335.
(28) Daldrop, P.; Reyes, F. E.; Robinson, D. A.; Hammond, C. M.; Lilley, D. M.; Batey, R. T.; Brenk, R. Novel Ligands for a Purine Riboswitch Discovered by RNA-Ligand Docking. *Chem. Biol.* **2011**, *18*, 324−335.
(29) Chen, L.; Cressina, E.; Leeper, F. J.; Smith, A. G.; Abell, C. A Fragment-Based Approach to Identifying Ligands for Riboswitches. *ACS Chem. Biol.* **2010**, *5*, 355−358.
(30) Warner, K. D.; Homan, P.; Weeks, K. M.; Smith, A. G.; Abell, C.; Ferré-D'Amaré, A. R. Validating Fragment-Based Drug Discovery for Biological RNAs: Lead Fragments Bind and Remodel the Tpp Riboswitch Specifically. *Chem. Biol.* **2014**, *21*, 591−595.
(31) Sung, H.-L.; Nesbitt, D. J. Sequential Folding of the Nickel/Cobalt Riboswitch Is Facilitated by a Conformational Intermediate: Insights from Single-Molecule Kinetics and Thermodynamics. *J. Phys. Chem. B* **2020**, *124*, 7348−7360.
(32) Sung, H. L.; Nesbitt, D. J. Novel Heat-Promoted Folding Dynamics of the Yybp-Ykoy Manganese Riboswitch: Kinetic and Thermodynamic Studies at the Single-Molecule Level. *J. Phys. Chem. B* **2019**, *123*, 5412−5422.
(33) Sung, H.-L.; Nesbitt, D. J. High Pressure Single-Molecule FRET Studies of the Lysine Riboswitch: Cationic and Osmolytic Effects on Pressure Induced Denaturation. *Phys. Chem. Chem. Phys.* **2020**, *22*, 15853−15866.
(34) Eschbach, S. H.; St-Pierre, P.; Penedo, J. C.; Lafontaine, D. A. Folding of the Sam-I Riboswitch: A Tale with a Twist. *RNA Biol.* **2012**, *9*, 535−541.
(35) Sung, H.-L.; Nesbitt, D. J. Single-Molecule FRET Kinetics of the Mn^{2+} Riboswitch: Evidence for Allosteric Mg^{2+} Control of "Induced-Fit" Vs "Conformational Selection" Folding Pathways. *J. Phys. Chem. B* **2019**, *123*, 2005−2015.
(36) Wilson, R. C.; Smith, A. M.; Fuchs, R. T.; Kleckner, I. R.; Henkin, T. M.; Foster, M. P. Tuning Riboswitch Regulation through Conformational Selection. *J. Mol. Biol.* **2011**, *405*, 926−938.
(37) Eskandari, S.; Prychyna, O.; Leung, J.; Avdic, D.; O'Neill, M. A. Ligand-Directed Dynamics of Adenine Riboswitch Conformers. *J. Am. Chem. Soc.* **2007**, *129*, 11308−11309.
(38) Suddala, K. C.; Walter, N. G. Riboswitch Structure and Dynamics by smFRET Microscopy. In *Riboswitch Discovery, Structure and Function*; Burke-Aguero, D. H., Eds.; Elsevier, 2014; Vol. *549*, pp 343−373.
(39) Roy, R.; Hohng, S.; Ha, T. A Practical Guide to Single-Molecule FRET. *Nat. Methods* **2008**, *5*, 507−516.
(40) Ma, B. Y.; Nussinov, R. Enzyme Dynamics Point to Stepwise Conformational Selection in Catalysis. *Curr. Opin. Chem. Biol.* **2010**, *14*, 652−659.
(41) St-Pierre, P.; McCluskey, K.; Shaw, E.; Penedo, J. C.; Lafontaine, D. A. Fluorescence Tools to Investigate Riboswitch Structural Dynamics. *Biochim. Biophys. Acta, Gene Regul. Mech.* **2014**, *1839*, 1005−1019.
(42) Blouin, S.; Chinnappan, R.; Lafontaine, D. A. Folding of the Lysine Riboswitch: Importance of Peripheral Elements for Transcriptional Regulation. *Nucleic Acids Res.* **2011**, *39*, 3373−3387.
(43) Blouin, S.; Lafontaine, D. A. A Loop Loop Interaction and a K-Turn Motif Located in the Lysine Aptamer Domain Are Important for the Riboswitch Gene Regulation Control. *RNA* **2007**, *13*, 1256−1267.
(44) Fiegland, L. R.; Garst, A. D.; Batey, R. T.; Nesbitt, D. J. Single-Molecule Studies of the Lysine Riboswitch Reveal Effector-Dependent Conformational Dynamics of the Aptamer Domain. *Biochemistry* **2012**, *51*, 9223−9233.
(45) McCluskey, K.; Boudreault, J.; St-Pierre, P.; Perez-Gonzalez, C.; Chauvier, A.; Rizzi, A.; Beauregard, P. B.; Lafontaine, D. A.; Penedo, J. C. Unprecedented Tunability of Riboswitch Structure and Regulatory Function by Sub-Millimolar Variations in Physiological Mg^{2+}. *Nucleic Acids Res.* **2019**, *47*, 6478−6487.
(46) Lemay, J. F.; Desnoyers, G.; Blouin, S.; Heppell, B.; Bastet, L.; St-Pierre, P.; Massé, E.; Lafontaine, D. A. Comparative Study between Transcriptionally- and Translationally-Acting Adenine Riboswitches Reveals Key Differences in Riboswitch Regulatory Mechanisms. *PLoS Genet.* **2011**, *7*, No. e1001278.
(47) Garst, A. D.; Héroux, A.; Rambo, R. P.; Batey, R. T. Crystal Structure of the Lysine Riboswitch Regulatory mRNA Element. *J. Biol. Chem.* **2008**, *283*, 22347−22351.
(48) Nicholson, D. A.; Sengupta, A.; Nesbitt, D. J. Chirality-Dependent Amino Acid Modulation of RNA Folding. *J. Phys. Chem. B* **2020**, *124*, 11561−11572.
(49) Nicholson, D. A.; Sengupta, A.; Sung, H. L.; Nesbitt, D. J. Amino Acid Stabilization of Nucleic Acid Secondary Structure: Kinetic Insights from Single-Molecule Studies. *J. Phys. Chem. B* **2018**, *122*, 9869−9876.
(50) Sengupta, A.; Sung, H.-L.; Nesbitt, D. J. Amino Acid Specific Effects on RNA Tertiary Interactions: Single-Molecule Kinetic and Thermodynamic Studies. *J. Phys. Chem. B* **2016**, *120*, 10615−10627.
(51) Aitken, C. E.; Marshall, R. A.; Puglisi, J. D. An Oxygen Scavenging System for Improvement of Dye Stability in Single-Molecule Fluorescence Experiments. *Biophys. J.* **2008**, *94*, 1826−1835.
(52) Holmstrom, E. D.; Nesbitt, D. J. Biophysical Insights from Temperature-Dependent Single-Molecule Förster Resonance Energy Transfer. *Annu. Rev. Phys. Chem.* **2016**, *67*, 441−465.
(53) Hennelly, S. P.; Novikova, I. V.; Sanbonmatsu, K. Y. The Expression Platform and the Aptamer: Cooperativity between Mg^{2+} and Ligand in the Sam-I Riboswitch. *Nucleic Acids Res.* **2013**, *41*, 1922−1935.
(54) Leipply, D.; Draper, D. E. Evidence for a Thermodynamically Distinct Mg^{2+} Ion Associated with Formation of an RNA Tertiary Structure. *J. Am. Chem. Soc.* **2011**, *133*, 13397−13405.
(55) Kinz-Thompson, C. D.; Bailey, N. A.; Gonzalez, R. L. Precisely and Accurately Inferring Single-Molecule Rate Constants. *Methods Enzymol.* **2016**, *581*, 187−225.
(56) Vander Meulen, K. A.; Davis, J. H.; Foster, T. R.; Record, M. T.; Butcher, S. E. Thermodynamics and Folding Pathway of Tetraloop Receptor-Mediated RNA Helical Packing. *J. Mol. Biol.* **2008**, *384*, 702−717.
(57) Wu, P.; Nakano, S.; Sugimoto, N. Temperature Dependence of Thermodynamic Properties for DNA/DNA and RNA/DNA Duplex Formation. *Eur. J. Biochem.* **2002**, *269*, 2821−2830.

https://doi.org/10.1021/acs.jpcb.1c07833
J. Phys. Chem. B XXXX, XXX, XXX−XXX

(58) Dupuis, N. F.; Holmstrom, E. D.; Nesbitt, D. J. Tests of Kramers' Theory at the Single-Molecule Level: Evidence for Folding of an Isolated RNA Tertiary Interaction at the Viscous Speed Limit. *J. Phys. Chem. B* **2018**, *122*, 8796−8804.
(59) Zwanzig, R.; Szabo, A.; Bagchi, B. Levinthal's Paradox. *Proc. Natl. Acad. Sci. U.S.A.* **1992**, *89*, 20−22.

https://doi.org/10.1021/acs.jpcb.1c07833
J. Phys. Chem. B XXXX, XXX, XXX−XXX